Shaping the Waveform of Entangled Photons

Alejandra Valencia,* Alessandro Ceré,† Xiaojuan Shi, Gabriel Molina-Terriza,‡ and Juan P. Torres§

ICFO-Institut de Ciencies Fotoniques, Mediterranean Technology Park, Castelldefels, 08860 Barcelona, Spain

(Received 7 June 2007; published 14 December 2007)

We demonstrate experimentally tunable control of the joint spectrum, i.e., waveform and degree of frequency correlations, of paired photons generated in spontaneous parametric down-conversion. This control is mediated by the spatial shape of the pump beam in type-I noncollinear configurations.

DOI: 10.1103/PhysRevLett.99.243601 PACS numbers: 42.50.Dv, 42.65.Lm

The joint spectrum of paired photons contains information about bandwidth, type of frequency correlations, and waveform of the two-photon state. The most appropriate form of the joint spectrum depends on the specific quantum optics application under consideration. For example, uncorrelated photon pairs can be used as a source of heralded single photons with a high degree of quantum purity [1,2]; the tolerance against mode mismatch in linear optical circuits can be enhanced by using photons with appropriately tailored waveform [3]; the use of frequency-correlated or anticorrelated photons allows erasing of the distinguishing information coming from the spectra when considering polarization entanglement [4,5]; some protocols for quantum enhanced clock synchronization and positioning measurements rely on the use of frequency anticorrelated [6] or correlated photons [7]. Moreover, frequency entanglement offers by itself a new physical resource to explore quantum physics in high-dimensional Hilbert space [8]. This requires the development of techniques to control the joint spectrum since it will allow generation of multidimensional waveform alphabets.

The most widely used method for generating entangled photon pairs is spontaneous parametric down-conversion (SPDC). Notwithstanding, paired photons with the desired joint spectrum may not be harvested directly at the output of the down-converting crystal. The question that arises is how to control independently different aspects of the joint spectrum of entangled paired photons generated in SPDC, importantly, the sought-after techniques that work for any frequency band of interest and any nonlinear crystal.

Various methods have been proposed and developed to control the type of frequency correlations and the bandwidth of down-converted photons. Some of them rely on an appropriate selection of the nonlinear crystal length and its dispersive properties [4,9]. Others are based on SPDC pumped by pulses with angular dispersion [10] or the design of nonlinear crystal superlattices [11]. Noncollinear SPDC has also been proposed as a way to tailor the waveform of the down-converted photons [12–17]. Contrary to the case of collinear SPDC, where the transverse spatial shape of the pump beam translates into specific features of the spatial waveform of the two-photon state, in noncollinear SPDC, the phase matching conditions inside the nonlinear crystal mediate the mapping of spatial features of the pump beam into the joint spectrum of the down-converted photons [18]. This spatial-to-spectral mapping allows one to tune independently frequency correlations and the waveform. In this Letter, we demonstrate experimentally this mapping and report experiments that demonstrate the feasibility of using noncollinear SPDC as a tool to control the type of frequency correlations using as tunable parameter the size of the pump beam waist and the angle of emission of the down-converted photons. In the past, measurements of the joint spectrum have been reported [5,19]. However, to the best of our knowledge this is the first time that manipulations of the joint spectrum have been demonstrated experimentally.

Consider noncollinear type-I SPDC in a nonlinear crystal of length L cut for noncritical phase matching. The quantum state of the two-photon pair can be written as $|\psi\rangle = \int d\Omega_s d\vec{q}_s d\Omega_i d\vec{q}_i \Phi(\Omega_s, \Omega_i, \vec{q}_s, \vec{q}_i)|\Omega_s, \Omega_i, \vec{q}_s, \vec{q}_i\rangle$, where $\Phi(\Omega_s, \Omega_i, \vec{q}_s, \vec{q}_i)$ is the mode function or biphoton, which contains all the information about the correlations and waveform properties of the two-photon light. $\Omega_j = \omega_j - \omega_j^0$ are frequency deviations from the central frequencies (ω_j^0), and $\vec{q}_j = (q_{jx}, q_{jy})$ are the transverse wave vectors for the signal (s) and idler (i) photons.

To elucidate the frequency correlations and waveform of the SPDC pairs, we consider the joint spectrum, $S(\Omega_s, \Omega_i) = |\int d\vec{q}_s d\vec{q}_i \Phi(\Omega_s, \Omega_i, \vec{q}_s, \vec{q}_i) U^*(\vec{q}_s) U^*(\vec{q}_i)|^2$, where the function $U(\vec{q}_j)$ describes the spatial mode in which the down-converted photons are projected, for instance, Gaussian modes when the down-converted photons are collected with an imaging system followed by single mode optical fibers [20,21]. Projection into large area modes is equivalent to projection into $\vec{q}_s = \vec{q}_i \simeq 0$, i.e., $U(\vec{q}) \propto \delta(\vec{q})$.

The down-converted photons travel inside the crystal at an angle $\varphi_s = -\varphi_i = \varphi$ with respect to the direction of propagation of the pump beam. The mode function can then be written as [22]

$$\Phi(\Omega_s, \Omega_i, \vec{q}_s, \vec{q}_i) = E_q(q_{xs} + q_{xi}, \Delta_0) E_\omega(\Omega_s + \Omega_i) \times \mathrm{sinc}\left(\frac{\Delta_k L}{2}\right) \exp\left\{i \frac{\Delta_k L}{2}\right\}, \quad (1)$$

where E_q and E_ω are the spatial shape of the pump beam in the transverse wave vector domain and the pump pulse frequency spectrum, respectively. $\Delta_0 = (q_{sy} + q_{iy}) \times \cos\varphi - (k_s + k_i)\sin\varphi$ accounts for the phase mismatching along the transverse direction, and $\Delta_k = k_p - (k_s + k_i) \times \cos\varphi - (q_{sy} + q_{iy})\sin\varphi$ for the phase matching conditions along the longitudinal direction. k_j (ω_j) is the wave vector for signal, idler, and pump waves. Equation (1) reveals that for the chosen configuration the spatial properties of the pump, E_q, are mapped into the spectral domain of the down-converted photons, $S(\Omega_s, \Omega_i)$, through the dependence of Δ_0 on the frequency.

To get further physical insight, we do a first-order Taylor expansion of $k_j(\omega_j^0 + \Omega_j)$ around the central frequencies, and assume large area collection modes ($\vec{q}_s = \vec{q}_i \simeq 0$). The joint spectrum reduces to

$$S(\Omega_s, \Omega_i) = |E_q(0, N_s \sin\varphi\Omega_-)|^2 |E_\omega(\Omega_+)|^2 \times \exp\left\{-\frac{[\alpha(N_p - N_s)\cos\varphi L]^2}{4}\Omega_+^2\right\}, \quad (2)$$

where $N_j \equiv dk_j/d\omega_j$ is the inverse group velocity, $\Omega_+ \equiv \Omega_s + \Omega_i$, and $\Omega_- \equiv \Omega_s - \Omega_i$. We have approximated the phase matching function, $\mathrm{sinc}(\Delta_k L/2)$, by an exponential function with the same width at the $1/e^2$ of the intensity: $\mathrm{sinc}(bx) \simeq \exp[-(\alpha b)^2 x^2]$, with $\alpha = 0.455$. Notice that the spatial-to-spectral mapping occurs between the shape of the pump beam along the transverse direction and the frequency shape in the Ω_- axis.

Figure 1 sketched the experimental setup used to demonstrate this mapping. A $L = 1$ mm $LiIO_3$ crystal, cut for type-I noncollinear degenerate SPDC, is pumped with a laser diode (Nichia NDHV220APAE1) centered at $\lambda_p^0 =$ 405 nm, with a measured bandwidth of $\Delta\lambda_p \simeq 0.4$ nm. The spatial mode of the laser beam is reduced to Gaussian by a set of cylindrical lenses and a spatial filter. The degenerate down-converted photons centered at $\lambda_s^0 = \lambda_i^0 = 810$ nm are produced at an internal angle $\varphi = 17.1°$ (which corresponds to noncritical phase matching) and are imaged into two single mode fibers via two lenses ($f =$ 11 mm) placed at 54 cm from the output face of the nonlinear crystal. The output of each fiber is sent through two monochromators (Jobin Yvon MicroHR), and finally sent into single photon counting modules (Perkin-Elmer SPCM-AQR-14-FC). Singles and coincidence counts for the two detectors are recorded and the joint spectrum is measured by scanning both monochromators.

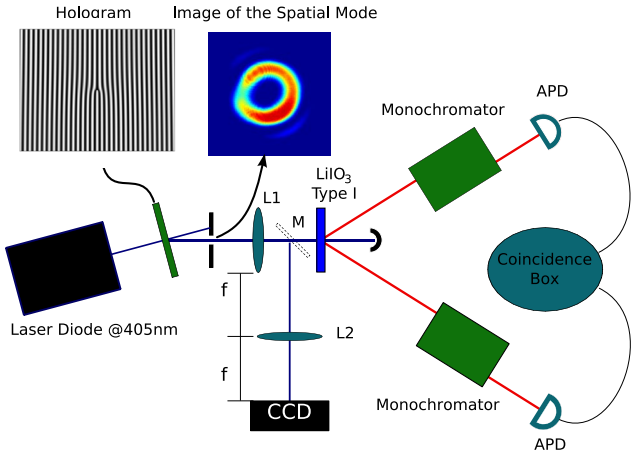

FIG. 1 (color online). Experimental setup. The Laguerre Gaussian mode is produced by a computer generated hologram. Photos of the hologram and the diffracted beam are shown. The beam size impinging into the crystal is controlled via $L1$. M is a flipping mirror used to switch from the frequency correlation measurement to the transverse momentum distribution measurement.

To recognize the spatial-to-spectral mapping, we choose pump spatial modes whose transverse wave number distributions possess a clearly identifiable dip in the center. The spatial profile of the pump beam is modified using two different schemes. First, we use a hologram that generates, into its second diffraction order, a vortex beam with topological charge $m = 2$. The hologram allows us to change from a Gaussian momentum distribution to a Laguerre Gaussian momentum distribution. After the hologram, there are various diffraction orders. An aperture is placed in such a way that only the second diffraction order arrives to the crystal. A picture of the hologram and the corresponding shape of the pump beam after the hologram are shown in the inset of Fig. 1. Alternatively, the pump beam is sent to a thin microscope slab that introduced a phase shift over half of the beam.

The transverse momentum distribution of the pump, $E_q(0, N_s \sin\varphi\Omega_-)$, which is the spatial shape to be compared with the joint spectrum of the down-converted photons, can be measured by means of the $2f$ system and a CCD camera. In the $2f$ system, we take into account the distance from the mirror to the entrance face of the nonlinear crystal ($\simeq$7 cm). The image from the camera relates to the frequency correlations according to $\Lambda_- = 4\pi y/(f N_s \sin\varphi\omega_s^0)$, where y is the spatial coordinate in the transverse direction and $\Lambda_- \equiv \lambda_s^0\Omega_-/\omega_s^0$.

Figure 2 compares the measured spatial shape of the pump beam in the transverse wave vector domain (solid line), $|E_q(0, N_s \sin\varphi\Omega_-)|^2$, and the measured joint spectrum shape as a function of Λ_- (dots). Figure 2(a) corresponds to the case when the pump beam shape is modified with the hologram, and Fig. 2(b) when the thin microscope slab is used. The matching of the solid lines and the points reveals the mapping of the pump's spatial characteristics, $E_q(0, N_s \sin\varphi\Omega_-)$, into the joint spectrum, $S(\Omega_s, \Omega_i)$. As a special feature, it is clear that the dip of the spatial pump profile translates into a dip in the joint spectrum at $\Lambda_- = 0$, i.e., $\lambda_s = \lambda_i = 810$ nm. Importantly, this technique makes it possible to tailor independently frequency waveform and type of correlations of the photon pairs.

The transferring of spatial characteristics of the pump beam into the joint spectrum of the down-converted pho-

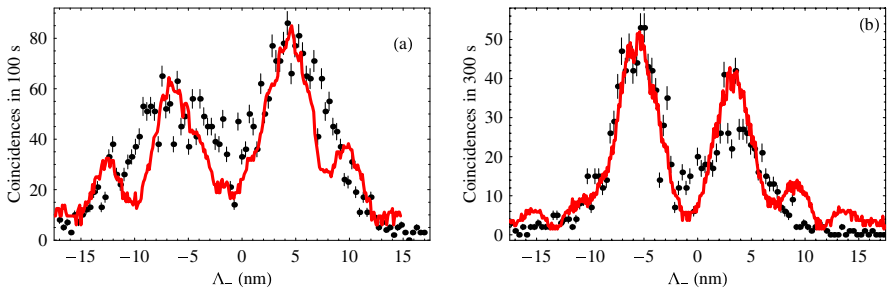

FIG. 2 (color online). Comparison of the measured spatial shape of the pump beam in the transverse wave vector domain (solid line) and the measured joint spectral intensity as a function of Λ_- (dots). The pump beam shape is modified with a hologram (a) and with a thin microscope slab (b).

tons, in principle, allows the control of the type of frequency correlations between signal and idler. Consider the case in which the pump beam is characterized by a transverse momentum profile $E(\vec{q}_p) \propto \exp[-|\vec{q}_p|^2 W_0^2/4]$ and a spectral distribution $E(\Omega_p) \propto \exp[-\Omega_p^2/(4B_p^2)]$. W_0 and B_p are the beam waist and the bandwidth of the pump beam. Furthermore, signal and idler are projected into the spatial mode $U(\vec{q}_j) \propto \exp[-|\vec{q}_j|^2 W_s^2/4]$. The joint spectrum then reads

$$S(\Omega_s, \Omega_i) = \mathcal{N} \exp\left\{-\frac{\Omega_+^2}{2B_+^2}\right\} \exp\left\{-\frac{\Omega_-^2}{2B_-^2}\right\}, \qquad (3)$$

where

$$B_- = \left[\frac{1}{2B_f^2} + \frac{(N_s \sin\varphi W_0)^2}{1 + 2(W_0 \cos\varphi / W_s)^2}\right]^{-1/2}, \qquad (4)$$

$$B_+ = \left[\frac{1}{B_p^2} + \frac{1}{2B_f^2} + \frac{(\alpha L)^2 (N_p - N_s \cos\varphi)^2}{1 + 2(\alpha \sin\varphi L / W_s)^2}\right]^{-1/2}, \qquad (5)$$

and $\mathcal{N}$ is a normalizing factor. We have also assumed the presence of frequency filters of the form $H(\Omega_{s,i}) \propto \exp[-\Omega_j^2/(4B_f^2)]$ in front of the detectors.

The ratio between the distribution widths B_+ and B_- characterizes the type of frequency correlation of the two-photon state: anticorrelated photons are obtained for W_0 so that $B_- \gg B_+$ and correlated photons when $B_- \ll B_+$. If $B_- = B_+$, we have uncorrelated frequency photons. From Eq. (4), the width B_- mainly depends on the pump beam width and the noncollinear angle. In order to compare with the experimental data, we will work with the variables Λ_- and $\Lambda_+ \equiv \lambda_s^0 \Omega_+ / \omega_s^0$ to which we associate the width (standard deviation) $\Delta\Lambda_-$ and $\Delta\Lambda_+$, respectively. Figure 3 shows the dependence of $\Delta\Lambda_-$ on the pump beam waist W_0 for different values of W_s. When for a value of W_s the $\Delta\Lambda_+$ and $\Delta\Lambda_-$ curves cross, we have the possibility of generating anticorrelated ($\Delta\Lambda_+ < \Delta\Lambda_-$), correlated ($\Delta\Lambda_+ > \Delta\Lambda_-$), and even uncorrelated ($\Delta\Lambda_+ = \Delta\Lambda_-$) frequency photons by choosing the appropriate value of the pump beam waist.

For the sake of clarity and due to the weak dependence of $\Delta\Lambda_+$ on W_s for a given pump bandwidth, we only plot $\Delta\Lambda_+$ for the ideal case, $W_s \to \infty$. When comparing the curves for different values of W_s, it is clear that the generation of anticorrelated photons is not greatly affected by the collection modes. Highly frequency anticorrelated photons are obtained for a focused pump and the relationship W_s/W_0 is large so that, effectively, one always projects into a large area mode and, therefore, approaches the condition $\vec{q}_s = \vec{q}_i \simeq 0$. On the other hand, the size of W_s sets a minimum value of the bandwidth of the pump for the generation of uncorrelated or highly correlated frequency two-photon states.

We demonstrate experimentally the feasibility of frequency correlation control with the setup of Fig. 1. We use a pump with a Gaussian profile and a telescope to modify the pump beam waist. W_0 is measured with a beam shaper (Coherent BM-7). For our collection scheme, the imaging relation give us a collection mode waist, $W_s^{\text{exp}} = 133.48\ \mu$m. The upper part of Fig. 4 shows the joint spectra, for two different values of W_0, obtained by scanning the two monochromators and recording coincidences. A two-dimensional Gaussian fit is used to obtain the bandwidths along Λ_+ and Λ_-. Figure 4(a) corresponds to the case of frequency anticorrelated photons while 4(b) corresponds to a two-photon state close to complete frequency uncorrelation. The measured bandwidths for Fig. 4(a) are $\Delta\Lambda_+ = 1.29$ nm and $\Delta\Lambda_- = 3.05$ nm, and for Fig. 4(b), $\Delta\Lambda_+ = 1.37$ nm and $\Delta\Lambda_- = 1.73$ nm.

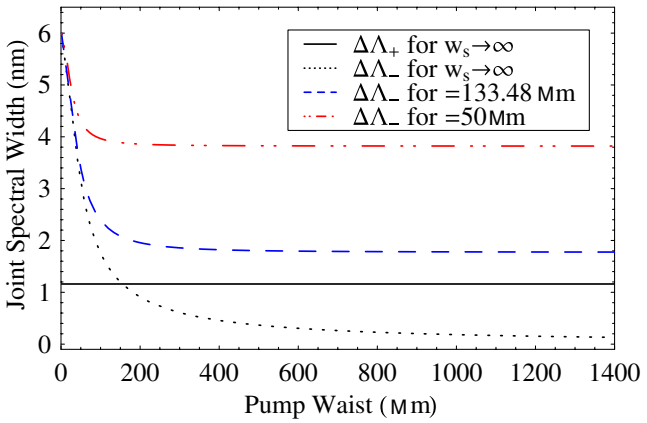

FIG. 3 (color online). Spectral widths $\Delta\Lambda_-$ and $\Delta\Lambda_+$ as a function of W_0. $\Delta\Lambda_-$ is shown for three different values of the spatial collection mode, $W_s = 133.48\ \mu$m, $W_s = 50\ \mu$m, and $W_s \to \infty$. $\Delta\Lambda_+$ is depicted only for $W_s \to \infty$. The intersection between $\Delta\Lambda_-$ and $\Delta\Lambda_+$ for $W_s \to \infty$ would allow complete tunable control of the type of frequency correlations.

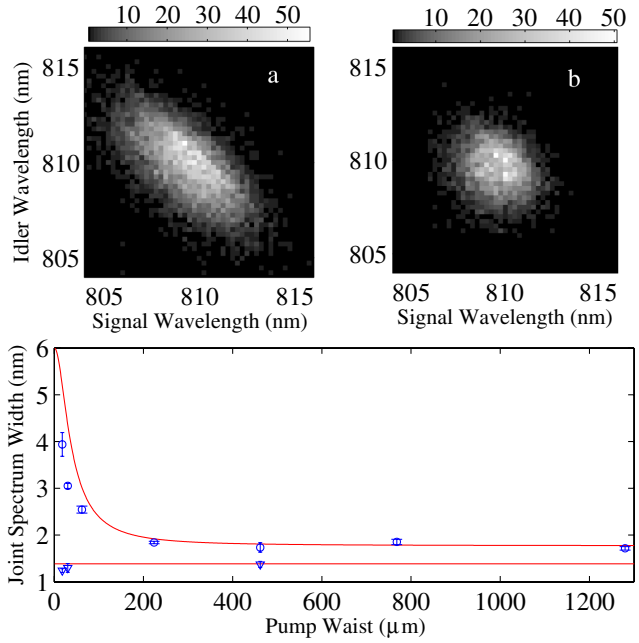

FIG. 4 (color online). (a),(b) depict two measured joint spectra: (a) for $W_0 = 30$ μm, each point is coincidences in 50 s; (b) for $W_0 = 462$ μm, each point is coincidences in 200 s. The lower part compares the theoretical prediction for the variation of $\Delta\Lambda_+$ and $\Delta\Lambda_-$ with W_0 with experimental values. In all cases, $W_s = 133$ μm.

The lower part of Fig. 4 compares the measured bandwidth for different pump beam waist with the theoretical prediction for our experimental parameters. From Eq. (4), one obtains that for large values of W_0, $\Delta\Lambda_- \rightarrow \lambda_s^0/\omega_s^0\sqrt{2}/(N_s \tan\phi W_s)$. Under our experimental conditions, this asymptotic value is $\Delta\Lambda_-^\infty = 1.77$ nm. On the other hand, the $\Delta\Lambda_+$ corresponding to the bandwidth of our pump laser is 1.38 nm. Therefore, the curves for $\Delta\Lambda_+$ and $\Delta\Lambda_-$ do not intersect, showing that our pump is not broad enough for achieving complete frequency-correlated photon pairs with our W_s.

In conclusion, we demonstrated experimentally the mapping of spatial characteristics imprinted on the pump beam into the joint spectrum of SPDC photons, and therefore, the generation of frequency shaped waveforms by spatially shaping the profile of the pump beam. Moreover, the use of spatial light modulators could allow the implementation of multidimensional waveform alphabets with any type of frequency correlations.

We have extended this capability and we have shown the feasibility of tunable control of frequency correlations of frequency-entangled two-photon states. The tuning parameter that mediates the control of the joint spectrum, and consequently the type of frequency correlations, is the spatial pump's beam waist. Changing this tuning parameter, we observed photons with a highly reduced degree of frequency correlation. The role of the spatial collecting mode and the bandwidth of the pump beam in the generation of highly correlated photon pairs was also explained.

The technique to control the frequency waveform reported here can be of great interest for enhancing waveform control of paired photons generated through two-photon Raman transitions in electromagnetically induced transparency schemes [23], where highly noncollinear geometries are frequently used [24]. In these configurations, a rudimentary control of the waveform is achieved by changing the Rabi frequency of a control laser. The mapping of spatial characteristics imprinted on the control laser beam into the joint spectrum might help to enhance such control.

This work is supported by EC under the integrated project Qubit Applications (QAP, IST directorate, Contract No. 015848), by Government of Spain (Consolider Ingenio 2010 QIOT No. CSD2006-00019 and No. FIS2004-03556), and by Generalitat de Catalunya.

*alejandra.valencia@icfo.es
†On leave from: Dipartimento di Fisica, Universitá di Camerino, I-62032 Camerino, Italy.
‡Also at: ICREA-Institucio Catalana de Recerca i Estudis Avancats, 08010 Barcelona, Spain.
§Also at: Department of Signal Theory and Communications, Universitat Politecnica de Catalunya, Barcelona, Spain.

[1] T. Aichele, A. I. Lvovsky, and S. Schiller, Eur. Phys. J. D **18**, 237 (2002).
[2] A. B. U'Ren *et al.*, Laser Phys. **15**, 146 (2005).
[3] P. P. Rohde, T. C. Ralph, and M. A. Nielsen, Phys. Rev. A **72**, 052332 (2005).
[4] W. P. Grice, A. B. U'Ren, and I. A. Walmsley, Phys. Rev. A **64**, 063815 (2001).
[5] H. S. Poh *et al.*, Phys. Rev. A **75**, 043816 (2007).
[6] A. Valencia, G. Scarcelli, and Y. Shih, Appl. Phys. Lett. **85**, 2655 (2004).
[7] V. Giovannetti, S. Lloyd, and L. Maccone, Nature (London) **412**, 417 (2001).
[8] C. K. Law, I. A. Walmsley, and J. H. Eberly, Phys. Rev. Lett. **84**, 5304 (2000).
[9] O. Kuzucu *et al.*, Phys. Rev. Lett. **94**, 083601 (2005).
[10] J. P. Torres *et al.*, Opt. Lett. **30**, 314 (2005).
[11] A. B. U'Ren *et al.*, Phys. Rev. Lett. **97**, 223602 (2006).
[12] Z. D. Walton *et al.*, Phys. Rev. A **67**, 053810 (2003).
[13] A. B. U'Ren, K. Banaszek, and I. A. Walmsley, Quantum Inf. Comput. **3**, 480 (2003).
[14] S. Carrasco *et al.*, Phys. Rev. A **73**, 063802 (2006).
[15] L. Lanco *et al.*, Phys. Rev. Lett. **97**, 173901 (2006).
[16] M. C. Booth *et al.*, Phys. Rev. A **66**, 023815 (2002).
[17] A. De Rossi and V. Berger, Phys. Rev. Lett. **88**, 043901 (2002).
[18] S. Carrasco *et al.*, Phys. Rev. A **70**, 043817 (2004).
[19] Y. H. Kim and W. P. Grice, Opt. Lett. **30**, 908 (2005).
[20] F. A. Bovino *et al.*, Opt. Commun. **227**, 343 (2003).
[21] C. Kurtsiefer, M. Oberparleiter, and H. Weinfurter, Phys. Rev. A **64**, 023802 (2001).
[22] J. P. Torres *et al.*, Opt. Lett. **29**, 1939 (2004).
[23] V. Balic *et al.*, Phys. Rev. Lett. **94**, 183601 (2005).
[24] P. Kolchin *et al.*, Phys. Rev. Lett. **97**, 113602 (2006).